Available online at www.sciencedirect.com
ScienceDirect
Nuclear Physics B Proceedings Supplement 00 (2014) 1–7
Nuclear Physics B Proceedings Supplement

Measurement of the Reactor Antineutrino Flux and Spectrum at Daya Bay

Weili Zhong, for the Daya Bay Collaboration

Institute of High Energy Physics, Beijing 100049, China

Abstract

Electron antineutrinos from six 2.9 GW_{th} reactors are detected with six detectors deployed in two near and one far underground experimental halls at Daya Bay. Using 217 days of data, more than 300,000 antineutrino candidates were detected in the three halls. In this talk, a measurement of absolute reactor antineutrino flux and spectrum is described, including comparisons of the measurement to predictions based on different reactor antineutrino flux models. A method for extracting a generic reactor antineutrino spectrum from the measured absolute antineutrino spectrum is presented, which could be used in place of current reactor antineutrino flux models.

Keywords: reactor antineutrino, absolute flux, absolute spectrum, Daya Bay

1. Introduction

The Daya Bay experiment detects reactor electron antineutrinos from six 2.9 GWth reactor cores at Daya Bay, Shenzhen in China, via inverse beta decay (IBD) interactions in functionally identical antineutrino detectors (ADs) at two near sites and one far site. A Near/far relative measurement is used to determine the neutrino mixing angle θ_{13}. In full operation, there are two ADs in the Daya Bay near site, two ADs in the LingAo near site, and four ADs in the far site. Full operation started on October 19, 2012. Before full operation, more than 300,000 IBD events were collected in the 6-AD data taking time (217 calendar days) from December 24, 2011 through July 28, 2012. The deployment of 6 ADs were two ADs in the Daya Bay near site, one AD in the LingAo near site, and three ADs in the far site. The IBD events collected in the 3 ADs of the two near sites in the 6-AD data taking time are used to report the measurement of absolute reactor antineutrino flux and spectrum. The ratio of measured to predicted flux is 0.947 ± 0.022 (0.992 ± 0.023) when normalized to the Huber[1] + Mueller[2] (ILL[3] + Vogel[4]) reactor antineutrino flux model. A measurement of absolute antineutrino spectrum with the candidates at the two near halls is also compared with spectra predicted by the Huber+Mueller and ILL+Vogel flux models. A generic reactor antineutrino spectrum is extracted from the absolute antineutrino spectrum for use in place of flux models to predict antineutrino spectra for future reactor antineutrino experiments.

2. Prediction of Reactor Antineutrino Flux and Spectrum

To compare the measurement of IBD events in the detectors with different flux models of reactor antineutrinos, detailed predictions of reactor antineutrino flux and spectrum are performed step by step, including the antineutrino spectrum produced at the reactors, neutrino oscillation from the reactors to the detectors, the detection efficiencies and energy response of detectors.
Antineutrino production during the fission process in reactor cores involves four primary isotopes: ^{235}U, ^{238}U, ^{239}Pu, and ^{241}Pu. Accordingly, the flux and spectrum of $\bar{\nu}_e$ from a reactor on a given day t can be predicted:

$$\frac{d^2N(E,t)}{dEdt} \equiv \sum_i \frac{W_{th}(t)}{\sum_j f_j(t)e_j} f_i(t) S_i(E) c_i^{ne}(E,t) + S_{SNF}(E,t) \quad (1)$$

where $W_{th}(t)$ is the reactor thermal power, $f_i(t)$ is the fission fraction of each isotope, e_i is the thermal

energy released per fission for each isotope, $S_i(E)$ is the $\bar{\nu}_e$ yield per fission for each of the four isotopes, $c_i^{ne}(E,t)$ is the correction to the yield due to reactor non-equilibrium effects, and $S_{SNF}(E,t)$ is the yield from spent nuclear fuel (SNF). Daily power $W_{th}(t)$ measurement and fission fraction $f_i(t)$ information from cycle simulation of reactor cores are offered by the nuclear power plant. Weekly $W_{th}(t)$ and $f_i(t)$ are deducted later for the prediction calculation. For the antineutrino spectrum of each isotope per fission $S_i(E)$, both older and newer models are used. In the older model, $S_i(E)$ of ^{235}U, ^{239}Pu, and ^{241}Pu are from the ILL experiment, and ^{238}U is from Vogel in the 1980s. In the newer model, $S_i(E)$ of ^{235}U, ^{239}Pu, and ^{241}Pu are from Huber, and ^{238}U is from Mueller et al. in 2011- 2012. The corrections of off-equilibrium and spent nuclear fuel (SNF) from the nearby SNF pool are also applied.
The uncertainty in reactor antineutrino rates has two categories: reactor correlated and reactor uncorrelated. Reactor correlated uncertainties are comprised of uncertainties in the fission energies of the four main isotopes [5] and in the antineutrino yield of each isotope $S_i(E)$[1][2][3][4]. Reactor uncorrelated uncertainties are comprised of uncertainties in the reactor power [8], fission fractions [9], SNF correction [6][7] and off-equilibrium correction [2]. The rate uncertainties are summarized in table 1 , where the IBD reaction

Table 1: Contributions of reactor related uncertainties

correlated		uncorrelated	
energy per fission	0.2%	power	0.5%
		fission fraction	0.6%
IBD reaction per fission	3%	spent fuel	0.3%
		off-equilibrium	0.3%
combined	3%	combined	0.9%

per fission is defined as the product of $S_i(E)$ and IBD cross-section $\sigma(E_\nu)$

$$\sigma_i \equiv \int_0^\infty S_i(E)\cdot\sigma(E)dE \qquad (2)$$

The main source of uncertainty in the reactor antineutrino spectrum is from the uncertainties in the isotope antineutrino spectra $S_i(E)$. The solid lines in figure 1 are the ratios of the antineutrino spectra predicted by the newer/older flux models for the three experimental sites. The gray band shows the relative uncertainties of the predicted spectra based on the flux models. The other contributors to spectral uncertainties are from fission fraction uncertainties, and SNF and off-equilibrium corrections. The 5% fission fraction uncertainties result

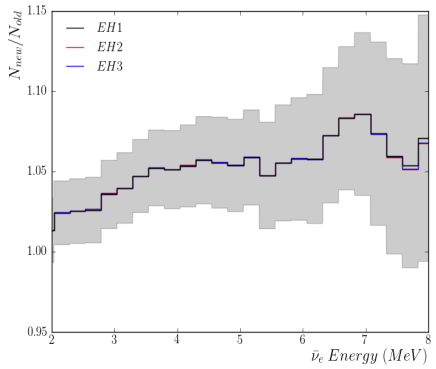

Figure 1: The ratios of predicted antineutrino spectrum with new and old flux models in each experimental hall without oscillation. Black, red and blue lines are the ratios at experimental hall (EH) 1, 2 and 3 respectively. The gray band represents the relative uncertainty of the isotope spectrum $S_i(E)$.

in a 0.6% – 1% uncertainty in each bin from low to high energy. The corrections due to SNF and off-equilibrium are less than 3% on each bin below 3.5 MeV. The spectral uncertainty of the corrections is conservatively assigned to be 100% in each bin.
When we detect electron antineutrinos at some distance away from the reactors, some electron antineutrinos change flavor due to neutrino oscillation. The survival probability of electron antineutrinos after traveling a distance L is

$$P(\bar{\nu}_e \to \bar{\nu}_e) \approx 1 - \sin^2 2\theta_{13}\sin^2(\frac{\Delta m^2_{ee}L}{4E_\nu}) - \cos^4\theta_{13}\sin^2 2\theta_{12}\sin^2(\frac{\Delta m^2_{21}L}{4E_\nu}) \qquad (3)$$

where $\sin^2 2\theta_{13} = 0.090^{+0.008}_{-0.009}$, and $|\Delta m^2_{ee}| = 2.59^{+0.19}_{-0.20}\times 10^{-3}eV^2$, which are the 6-AD oscillation analysis results of Daya Bay using the same data set[10]. The other two oscillation parameters are from PDG 2012.
After the consideration of oscillation probability, the last step of the prediction is to convert the antineutrino spectrum $S(E_{\bar{\nu}_e})$ into a prompt spectrum $S(E_{e^+})$ of IBD events as collected in the detectors. The conversion process can be written as

$$S(E_{e^+}) = S(E_{\bar{\nu}_e})\cdot\sigma_{IBD}(E_{\bar{\nu}_e})\cdot N_P\cdot t_{live}\cdot\epsilon_{m\cdot\mu}\cdot\epsilon\cdot DetRes \qquad (4)$$

where $S(E_{\bar{\nu}_e})$ is the spectrum of reactor antineutrinos at one detector of one near site from all six reactor cores, after the application of oscillation probabilities; $\sigma_{IBD}(E_{\bar{\nu}_e})$ is the IBD cross section; N_P is the target proton number in one detector; t_{live} is the live time of one

near site during the 217 calendar days; $\epsilon_{m\cdot\mu}$ is the product of the muon veto efficiency and the efficiency of the multiplicity cut for IBD event selection, both for one near site; and ϵ is the absolute detection efficiency of the detectors. Table 2 summarizes the absolute detection efficiency and its uncertainties. The absolute detector efficiency is obtained from detector Monte Carlo (MC) simulation which is tuned with various data. The uncertainty in detection efficiency is 2.1%, which is obtained after improved evaluation regarding the delayed energy cut, Gd capture ratio and spill-in effect. 'DetRes' is the energy response of the detectors, which is important for

Table 2: Summary of absolute efficiencies and absolute systematic uncertainties. The uncertainties are given in relative units.

	Efficiency	Uncertainty
Target protons		0.47%
Flasher cut	99.98%	0.01%
Delayed energy cut	92.71%	0.97%
Prompt energy cut	99.81%	0.10%
Muon veto cut	-	0.02%
Multiplicity cut	-	0.02%
Capture time cut	98.70%	0.12%
Gd capture ratio	84.17%	0.95%
Spill-in correction	104.86%	1.50%
Combined	80.59%	2.08%

predicting the prompt spectrum of IBD events properly and comparing it with the measurement. The detector response matrix is obtained with two primary methods. One method is adding detector effects step-by-step: energy losses (energy deposited in acrylic rather than scintillator, etc.) → nonlinear energy response of the detector → energy smearing due to detector energy resolution. The other method is a full detector MC simulation. For both methods, the dominant spectral uncertainty is

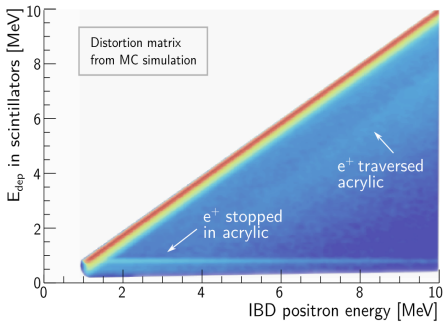

Figure 2: Energy losses in acrylic vessels, obtained from Geant4 MC simulation.

from the uncertainty in nonlinear energy response. For the three-step method, energy losses are obtained via detector simulation in Geant4 without optical processes (figure 2), so the deposited energy could be related to the initial energy of an IBD positron. The nonlinear energy response is due to the quenching and Cherenkov light effects in the liquid scintillator, and the nonlinear response of the electronics due to the charge integration and time window. The nonlinear response curve is obtained by an unconstrained fit of calibration data from gamma sources and ^{12}B data. As shown in figure 3, the uncertainty in nonlinearity response is less than 1%. With the nonlinearity curve of E_{vis}/E_{true} versus E_{true}, the true (initial) energy of an IBD positron is converted into a visible energy in the detector. The

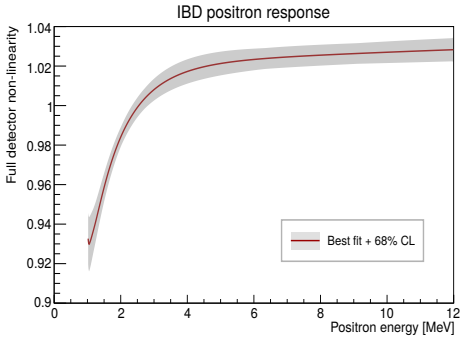

Figure 3: Nonlinear energy response, obtained by an unconstrained fit of gamma calibration and ^{12}B data.

energy resolution of Daya Bay antineutrino detectors is about $8.4\%/\sqrt{E(MeV)}$, as shown in figure 4, and is determined with gamma events from gamma and neutron sources placed at the center of detectors, and also by gamma events from the capture of IBD and spallation neutrons, which are uniformly distributed inside the Gd-doped liquid scintillator region. After the three steps, the predicted visible energy spectrum of IBD prompt signals $S(E_{\bar{\nu}_e})$ is obtained.

3. Absolute Flux Measurement

To obtain the absolute flux, the rate-only oscillation fitter in [11] is slightly modified:

$$\chi^2 = \sum_{d=1}^{6} \frac{[M_d - T_d(1+\epsilon_R+\epsilon_D+\sum_r \omega_r^d \alpha_r + \epsilon_d) + \eta_d]^2}{M_d + B_d} + \sum_r \frac{\alpha_r^2}{\sigma_r^2} + \sum_{d=1}^{6}\left(\frac{\epsilon_d^2}{\sigma_d^2} + \frac{\eta_d^2}{\sigma_B^2}\right) + \frac{\epsilon_D^2}{\sigma_D^2} \quad (5)$$

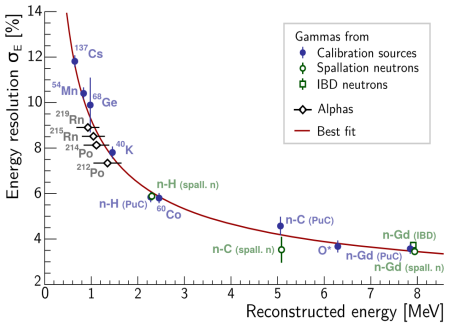

Figure 4: Energy resolution obtained with gamma data from calibration sources, IBD neutrons and spallation neutrons, all corrected for detector non-uniformity.

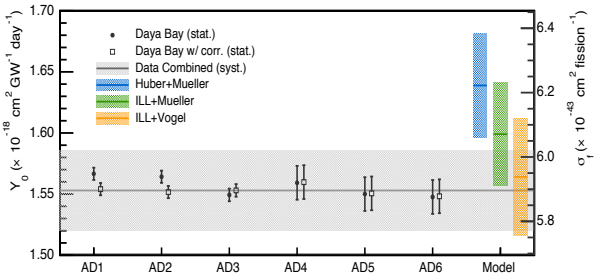

Figure 5: Absolute IBD yields (black dots and circles: measured IBD yield Y_0 and σ_f at each AD. Circles are the results after the corrections of reactor power and fission fraction differences of six cores. The error bars on dots and circles are statistical errors. The gray band is systematical error, including reactor- and detector-related uncertainties. The colored bars are the predicted IBD yield Y_0 and σ_f with different reactor flux models.

where the M_d are the measured IBD events of the dth detector with backgrounds subtracted, the B_d are the corresponding backgrounds of each detector, the T_d are the predicted IBD events from the flux prediction, MC detector response and neutrino oscillation, as described in section 2, except that $\sin^2 2\theta_{13}$ is a fitting parameter; and ω_r^d is the fractional IBD contribution from the rth reactor to the dth detector determined by baselines and reactor fluxes. σ_r (0.9%) is the uncorrelated reactor uncertainty, σ_d (0.2%) is the uncorrelated detection efficiency uncertainty, and σ_B is the background uncertainty. α_r, ϵ_d and η_d are the corresponding nuisance parameters. The nuisance parameter ϵ in the original fitter is separated into two terms, ϵ_R and ϵ_D, where ϵ_R is the nuisance parameter for the reactor flux absolute normalization, and is left free floating. ϵ_D is for the absolute uncertainty of the detection efficiency, with a penalty term added into the fitter based on its uncertainty. The two free parameters are $\sin^2 2\theta_{13}$ and ϵ_R. Using the the ILL+Vogel (Huber+Mueller) model in the prediction, the best-fit results are $\sin^2 2\theta_{13}$ = 0.0905 ± 0.0095 ($\sin^2 2\theta_{13}$ = 0.0906 ± 0.0095), ϵ_R = -0.007 ± 0.023 (ϵ_R = -0.053 ± 0.022). The effect on $\sin^2 2\theta_{13}$ when using different models is negligible. The measurement over prediction ratio is (1-ϵ_R); i.e., 0.993 ± 0.023 (0.947 ± 0.022) if normalized to the ILL+Vogel (Huber+Mueller) flux model. The uncertainty in ϵ_R is dominated by the uncertainty in absolute detection efficiency (2.1%). The other sources of uncertainty are statistical (0.2%), $\sin^2 2\theta_{13}$ (0.2%), and reactor-related (0.9%). In addition, when the ^{238}U isotope spectrum is replaced by the latest measurement of the Munich group [12] in the Huber+Mueller model, the change of measurement over prediction ratio is negligible.

Another way to obtain the absolute antineutrino flux without a fitter is to directly normalize the measured IBD yield in each detector after background subtraction to a unit of $cm^2/GW/Day$, which is defined as Y_0, or to a unit of $cm^2/fission$, i.e. σ_f. Figure 5 shows the measured flux of each detector in the two units and compares them with the predicted fluxes of different reactor flux models. Y_0 and σ_f from the combined IBD measurement of the 3 ADs of the two near sites are 1.553×10^{-18} and 5.934×10^{-43}, respectively. The effective baseline is 573 m, which is calculated with the flux weighted detector-reactor distances of the 3 ADs. The effective fission fractions ^{235}U : ^{238}U : ^{239}Pu : ^{241}Pu = 0.586 : 0.076 : 0.288 : 0.050 are also for the 3 ADs in two near sites. Figure 6 shows the global ratio of measurement over prediction (with Huber + Mueller model) from previous experiments with the normalization method used in [13], where the global ratio R is 0.943±0.008(exp). The Daya Bay measurement (R = 0.947±0.022) is consistent with previous short baseline experiments.

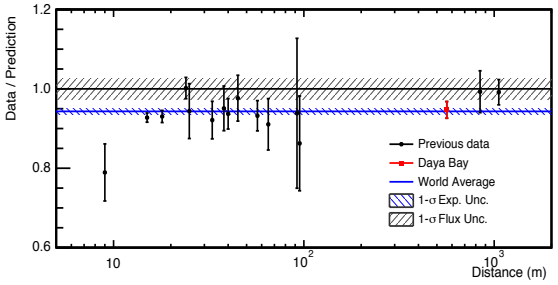

Figure 6: The measured antineutrino flux from experiments with various baselines, normalized to the Huber+Mueller flux model. The horizontal bar represents the global average and its 1σ error band. The 3% reactor flux uncertainty is shown as a band around unity.

4. Absolute Spectrum Measurement

The measured prompt spectra of IBD events in the three ADs of the two near sites are combined and compared with predictions. The predictions are obtained using both Huber+Mueller model and ILL+Vogel models. The procedure of obtaining a predicted IBD prompt spectrum in one detector is described in sec 2. For spectrum-only comparison, the predicted spectra are normalized to the measured spectrum. To test the consistency between the measurement and predictions, a full covariance matrix is used to calculate the χ^2:

$$\chi^2 = (N_i^{obs} - N_i^{pred})V_{ij}^{-1}(N_j^{obs} - N_j^{pred})$$
$$V = V_{stat} + V_{reactor} + V_{detector} + V_{bkgs} \quad (6)$$

where N_i^{obs} is event number of the ith bin of the measured prompt spectrum, and N_i^{pred} is event number of the ith bin of the predicted prompt spectrum after normalization. The energy range of the prompt spectrum is from 0.7 to 12 MeV, 25 bins in total. There is one bin for 0.7-1.25 MeV, one bin for 7-12 MeV, and 23 bins from 1.25-7 MeV. The 0.25 MeV bin width in 2-7 MeV is for the convenience of comparison with prediction. There is only one bin above 7 MeV because of the small amount of data. Since there is no prediction from flux models above 8 MeV in antineutrino energy, the prediction in this region is from extrapolation. NDF is the number of bins minus one due to normalization, i.e. 24. The full covariance matrix V is composed of the covariance matrices of statistical, systematic (reactor- and detector-related) and background uncertainties. The diagonal elements of the full covariance matrix and its components are shown in figure 7. Figure 8 shows the comparison of the measured and

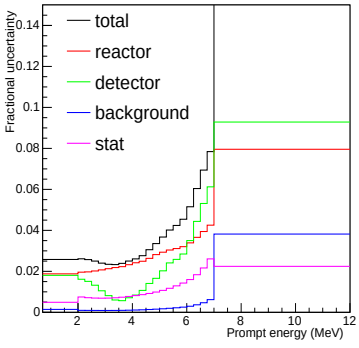

Figure 7: Diagonal elements of the full covariance matrix and its components.

predicted IBD prompt spectrum. The absolute spectra are shown in the top pad. The black dots are the measurement with statistical error bars. The red dots are the prediction with the Huber+Mueller model, normalized to the measurement. To see the difference between measurement and prediction more clearly, the ratio of the measurement and the prediction is shown in the bottom pad. The gray band contains the diagonal elements of $V_{reactor}$, and the red band contains the diagonal elements of the full covariance matrix, excluding statistical errors. There is deviation between measurement and prediction, particularly in 4-6 MeV, as other reactor experiments have also reported [14][15]. A χ^2 comparison between model and measurement in the full range of 0.7-12 MeV using the full covariance matrix yields χ^2/ndf = 41.4/24, which corresponds to a 2.4σ discrepancy. The flat shape of blue curve which is the ratio of two predictions with different flux models shows that there is also deviation between measurement and prediction with the ILL+Vogel model. In the oscillation

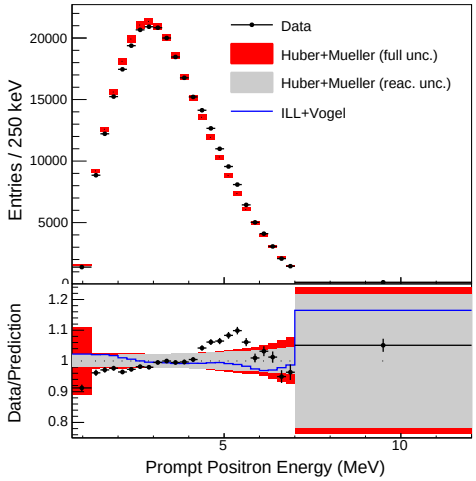

Figure 8: Comparison of measured and predicted IBD prompt spectrum of the 3 ADs in the two near sites. Top pad: the absolute spectra of measurement and prediction (Huber+Mueller model). Bottom pad: Ratio of measurement and prediction (Huber+Mueller model) and uncertainty band. The blue curve is the ratio of prediction with the ILL+Vogel model over prediction with the Huber+Mueller model.

analysis for $\sin^2 2\theta_{13}$, the χ^2/ndf is 134.7/146, which means the shapes of the IBD prompt spectra among detectors at the near and far sites are very consistent, in contrast to the shapes of measurement and prediction, which are inconsistent. To quantify the significance of localized deviations, two methods are developed. One method is the χ^2 contribution from each bin, which is

evaluated by:

$$\widetilde{\chi_i} = \frac{N_i^{obs} - N_i^{pred}}{|N_i^{obs} - N_i^{pred}|} \sqrt{\frac{1}{2}\sum_j (\chi_{ij}^2 + \chi_{ji}^2)} \quad (7)$$

$$\text{where } \chi_{ij}^2 = (N_i^{obs} - N_i^{pred}) V_{ij}^{-1} (N_j^{obs} - N_j^{pred})$$

and shown in pad (b) of figure 9. The other method is to scan the spectrum with a fixed window within which N nuisance parameters with no penalty terms are introduced to the fitter of the spectral analysis, where N is the number of bins within the window. The χ^2 difference before and after introducing the N nuisance parameters follows a χ^2 distribution with NDF = N-1, from which we obtain the P-value. Pad (c) of figure 9 shows a P-value scan using a 1 MeV window (N=4 for a 0.25 MeV bin-width). In the 2 MeV window at [4, 6], the P-value is 4.66×10^{-5}, i.e. a 4.1σ discrepancy. The local discrepancies between data and predictions with different reactor flux models are similar. The measured events in 4-6 MeV are found to be time-independent and power correlated like other IBD events. Moreover, the events in this energy range have characteristics which are consistent with IBD events; namely, consistent distributions of neutron capture time, vertex position, distance between prompt and delayed vertexes, etc. This, coupled with the fact that no anomalies are seen in other data samples such as ^{12}B continuous spectra, strongly disfavors an explanation involving the detector response or an unknown background. The latest ab-initio calculation of the antineutrino spectrum of fission isotopes with all beta-decay branch information from a nuclear database identifies prominent fission daughter isotopes as a possible origin for the discrepancy in the 4-6 MeV energy region [16].

5. Observable Reactor Antineutrino Spectrum

Since significant discrepancy exists between data and prediction, it is useful to extract a generic reactor antineutrino spectrum that is independent to the specific detector response of the Daya Bay experiment. The generic antineutrino spectrum therefore could be used for flux and spectrum predictions by other reactor antineutrino experiments, or for comparison with reactor antineutrino flux models. The first step is to unfold the IBD prompt spectrum, which is a combination of the measurements of the three ADs of the two near sites. With the input of the detector response matrix from full detector MC simulation, and the measured IBD prompt spectrum and its covariance matrix, an unfolded antineutrino spectrum is obtained via multiple unfolding

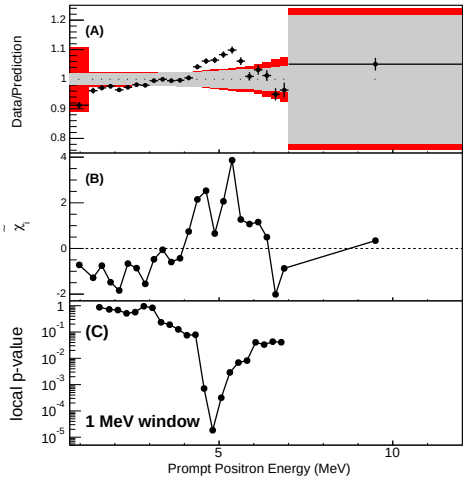

Figure 9: (a). Spectrum comparison of data and prediction, same as figure8. (b). χ^2 contribution of each bin. (c). P-value scan of $\delta\chi^2$/NDF with a 1 MeV energy window.

methods, such as Singular Value Decomposition (SVD) and Bayes iteration [17][19][18]. The generic antineutrino spectrum is obtained by removing the oscillation effect from the unfolded spectrum and normalizing the unfolded spectrum to $cm^2/fission/MeV$:

$$S_{obs}(E_{\bar{\nu}_e}) = \frac{S_{unfolded}(E_{\bar{\nu}_e})}{P_{eff}(E_{\bar{\nu}_e}, L) \cdot N_P \cdot F_{total}} \quad (8)$$

where N_P is the proton number in unit target mass; $P_{eff}(E_{\bar{\nu}_e}, L)$ is the survival probability of electron antineutrinos which is weighted by the fluxes from the six cores; F_{total} is the total number of fissions in all six cores. The top pad of figure 10 shows the generic antineutrino spectrum from Daya Bay. For comparison, the predicted spectrum in the same units given by equation 9, is also shown in the top pad of figure 10:

$$S_{pred}(E_{\bar{\nu}_e}) = (\sum_k \alpha_k S_k(E) + c^{ne}(E) + SNF(E)) \cdot \sigma_{IBD}(E) \quad (9)$$

where α_k are the effective fission fractions of Daya Bay which are given in section 3. Since the generic antineutrino spectrum includes the IBD cross-section, it is referred to as an 'observable' reactor antineutrino spectrum. The bottom pad of figure 10 is the ratio of the measured and predicted observable reactor antineutrino spectrum. It shows the same rate deficit as the flux measurement and similar spectral deviations as in the comparison of measured and predicted IBD prompt spectra. The observable antineutrino spectrum of Daya Bay also supplies data outside [2, 8] MeV, while the uncertainties are undergoing further investigation.

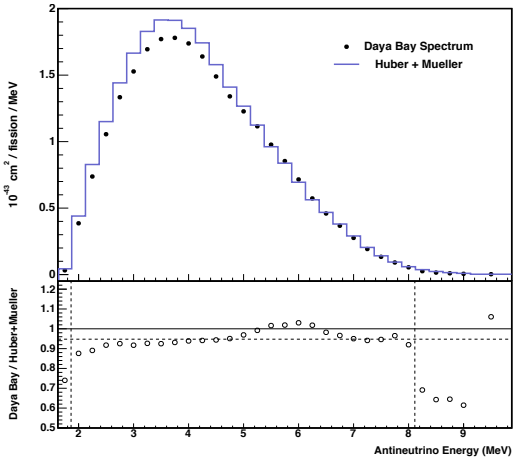

Figure 10: Top pad: data points represent the observable reactor antineutrino spectrum from the measurement of Daya Bay. The blue curve is the predicted spectrum with the Huber+Muellller model. Bottom pad: ratio of the Daya Bay measurement and the Huber+Mueller prediction. The horizontal dashed line is at 0.947, when normalizing the Daya Bay measurement to the Huber+Mueller model. Two vertical dashed lines signify that, outside [2, 8] MeV, the predicted spectrum with the Huber+Mueller model is from extrapolation.

6. Summary

A measurement of the reactor antineutrino flux and spectrum from the Daya Bay experiment is reported, with about 300,000 IBD events collected in the three ADs of the two near sites. The absolute flux measurement is consistent with previous short baseline measurements. The ratio of measurement over prediction with the Huber+Mueller (ILL+Vogel) model is R = 0.947 ± 0.022 (0.993 ± 0.023). The IBD positron spectrum measurement is not consistent with current reactor antineutrino flux models, where the deviation in 4-6 MeV is about 4σ. Investigation of IBD candidates inside this energy region shows that the events are reactor power-correlated as other IBD events. Considering the discrepancies between the measurement and predictions, a generic observable reactor antineutrino spectrum is extracted from the measured positron spectrum of Daya Bay. Uncertainties of unfolding are undergoing investigation. In the future, the measurements will be updated with 6+8 AD data, and uncertainties in detection efficiency are expected to be further improved.

References

[1] P. Huber, Phys. Rev. C 84, 024617 (2011), 85, 029901(E) (2012).
[2] T. Mueller *et al*. Phys. Rev. C 83, 054615 (2011).
[3] K. Schreckenbach *et al*. Phys. Lett. B. 160, 325 (1985), F. von Feilitzsch, A. A. Hahn and K. Schreckenbach, Phys. Lett. B. 118, 162 (1982), A. A. Hahn *etal*. Phys. Lett. B 218, 365 (1989).
[4] P. Vogel, G. K. Schenter, F. M. Mann, and R. E. Schenter, Phys. Rev. C 24, 1543 (1981).
[5] V. Kopeikin, L. Mikaelyan, and V. Sinev, Phys. At. Nucl. 67, 1892 (2004).
[6] F. P. An, X. C. Tian, L. Zhan, and J. Cao, Chin. Phys. C 33, 711 (2009).
[7] B. Zhou, X. C. Ruan, Y. B. Nie, Z. Y. Zhou, F. P. An, and J. Cao, Chin. Phys. C 36, 1 (2012).
[8] J. Cao, Nuclear Physics B (Proc. Suppl.) 229-232 (2012) 205-209 [arXiv:11012266]
[9] APOLLO2: Vailidation/Qualification http://nucleaire-saclay.cea.fr/Phocea/Vie_des_labos/Ast/ast_technique.php?id_ast=351
[10] F. P. An *et al*. (Daya Bay Collaboration), Phys. Rev. Lett. 112, 061801(2014).
[11] F. P. An *et al*. (Daya Bay Collaboration), Phys. Rev. Lett. 108, 171803 (2012).
[12] N. Haag *et al*., arXiv:1312.5601.
[13] C. Zhang, X. Qian, and P. Vogel, Phys. Rev. D 87, 073018 (2013).
[14] Y. Abe, J. C. dos Anjos, *et. al*. (Double Chooz Collaboration), arXiv: 1406.7763v2.
[15] Reno Collaboration, talk at Neutrino 2014
[16] D. A. Dwyer, T. J. Langford, arXiv:1407.1281.
[17] http://hepunx.rl.ac.uk/~adye/software/unfold/RooUnfold.html
[18] G. D'Agostini, Nucl. Inst. Meth. A 362, 487 (1995)
[19] Höcker and Kartvelishvili, Nucl. Inst. Meth. A 372, 469 (1996)